minerals

MDPI

Article

Spontaneous Serpentine Carbonation Controlled by Underground Dynamic Microclimate at the Montecastelli Copper Mine, Italy

Chiara Boschi [1,*], Federica Bedini [1], Ilaria Baneschi [1], Andrea Rielli [1], Lukas Baumgartner [2], Natale Perchiazzi [3], Alexey Ulyanov [2], Giovanni Zanchetta [3] and Andrea Dini [1]

1 Istitute of Geoscience and Earth Resources, National Research Council of Italy (CNR), 56100 Pisa, Italy; kicca1000@hotmail.it (F.B.); ilaria.baneschi@igg.cnr.it (I.B.); andrea.rielli@igg.cnr.it (A.R.); andrea.dini@igg.cnr.it (A.D.)

2 Institute of Earth Sciences, University of Lausanne, Geopolis Building, CH-1015 Lausanne, Switzerland; Lukas.Baumgartner@unil.ch (L.B.); Alexey.Ulyanov@unil.ch (A.U.)

3 Earth Sciences Department, Pisa University, Via S. Maria 53, I-56126 Pisa, Italy; natale.perchiazzi@unipi.it (N.P.); zanchetta@dst.unipi.it (G.Z.)

* Correspondence: chiara.boschi@igg.cnr.it

Received: 15 October 2019; Accepted: 5 December 2019; Published: 18 December 2019

Abstract: Understanding low temperature carbon sequestration through serpentinite–H_2O–CO_2 interaction is becoming increasingly important as it is considered a potential approach for carbon storage required to offset anthropogenic CO_2 emissions. In this study, we present new insights into spontaneous CO_2 mineral sequestration through the formation of hydromagnesite + kerolite with minor aragonite incrustations on serpentinite walls of the Montecastelli copper mine located in Southern Tuscany, Italy. On the basis of field, petrological, and geochemical observations coupled with geochemical modeling, we show that precipitation of the wall coating paragenesis is driven by a sequential evaporation and condensation process starting from meteoric waters which emerge from fractures into the mine walls and ceiling. A direct precipitation of the coating paragenesis is not compatible with the chemical composition of the mine water. Instead, geochemical modeling shows that its formation can be explained through evaporation of mine water and its progressive condensation onto the mine walls, where a layer of serpentinite powder was accumulated during the excavation of the mine adits. Condensed water produces a homogeneous film on the mine walls where it can interact with the serpentinite powder and become enriched in Mg, Si, and minor Ca, which are necessary for the precipitation of the observed coating paragenesis. The evaporation and condensation processes are driven by changes in the air flow inside the mine, which in turns are driven by seasonal changes of the outside temperature. The presence of "kerolite", a Mg-silicate, is indicative of the dissolution of Si-rich minerals, such as serpentine, through the water–powder interaction on the mine walls at low temperature (~17.0 to 18.1 °C). The spontaneous carbonation of serpentine at low temperature is a peculiar feature of this occurrence, which has only rarely been observed in ultramafic outcrops exposed on the Earth's surface, where instead hydromagnesite predominantly forms through the dissolution of brucite. The high reactivity of serpentine observed, in this study, is most likely due to the presence of fine-grained serpentine fines in the mine walls. Further study of the peculiar conditions of underground environments hosted in Mg-rich lithologies, such as that of the Montecastelli Copper mine, can lead to a better understanding of the physical and chemical conditions necessary to enhance serpentine carbonation at ambient temperature.

Keywords: CO_2 mineral sequestration; hydromagnesite; kerolite; serpentinite; Cu mine; Montecastelli; underground microclimate

1. Introduction

The formation of hydromagnesite ($Mg_5(CO_3)_4(OH)_2{\cdot}4H_2O$) is generally associated with low-temperature alteration of ultramafic rocks and has attracted an increasing number of studies because during its formation CO_2 is chemically bound within its structure, representing a natural analogue of CO_2 mineral sequestration [1–7]. The study of natural CO_2 sequestration through the formation of carbonate from ultramafic rocks can help developing more efficient engineered CO_2 storage processes involving both *in situ* and *ex situ* approaches, which are necessary to mitigate anthropogenic CO_2 emissions [8]. Southern Tuscany offers several examples of spontaneous low- and high-temperature carbonation of ultramafic rocks [1,9]. Boschi et al., (2017) showed the presence of hydromagnesite and layered double hydroxides (LDH) in association with serpentinized dunite that outcrops nearby the Montecastelli Cu mine. The authors highlighted that the efficiency of carbonation was linked to the substratum lithology on which the carbonation processes took place. The most efficient reactions were found to occur on serpentinized dunites that are rich in brucite. Brucite is preferentially dissolved at surficial conditions as compared with serpentine, producing a Mg-rich fluid necessary for the precipitation of hydromagnesite [1]. Due to the lithological selectivity of the process, only brucite-rich dunite bodies showed significant carbonation with the formation of hydromagnesite and LDH at the outcrop scale. In this study, we focus on hydromagnesite formation (+ kerolite and aragonite) in adits of the Montecastelli Cu mine. We show that the formation of hydromagnesite in an underground environment is triggered by a different process as compared with the surface, which consists of a complex interaction between meteoric water percolation, evaporation and condensation, and interaction with serpentinite fines accumulated on the adits' walls.

2. Geological Background and Topographic-Microclimatic Characteritics of the Mine

Southern Tuscany is characterized by several outcrops of ultramafic and mafic rocks belonging to the Ligurian units. These comprise serpentinized harzburgites and dunites, gabbros and basalts, with their original sedimentary cover [1,9–11]. A large ophiolite body outcrops near the village of Montecastelli Pisano. Here, the Pavone river has eroded a canyon through the ultramafic units exposing outcrops of harzburgite and dunite which locally have been strongly carbonated [1]. The Montecastelli ultramafic body has been affected by the following two main stages of deformation: (i) early ductile shearing recorded by mylonitic gabbros and (ii) late brittle deformation with the development of cataclastic zones and the recrystallization of serpentinite-gabbro-basalt assemblage. A major cataclastic zone, which runs through the entire ultramafic body WNW–ESE, hosts a reworked Cu-Fe sulphide mineralization, mainly represented by bornite, chalcopyrite, and chalcocite in veins and nodules [12–14]. The deposit was intermittently explored and mined between 1832 and 1942 through the excavation of small open pits and underground works, providing a negligible, total production of 40 tons of Cu-Fe sulphides.

The Montecastelli copper mine (43°16.4′ N; 10°56.7′ E) consists of about 1500 m of adits and drifts distributed over three levels from 195 m to 245 m above sea level (a.s.l.) connected by a main shaft and smaller inclined shafts (Figure 1). The three main adits have been excavated in serpentinized harzburgite and dunite reaching a NW-trending mineralized cataclastic zone from which the surface (ca. 320 m a.s.l.) plunges towards NE. The upper part of the cataclastic zone (from 320 m down to 245 m) is poorly mineralized and there are no underground works directly connecting the uppermost exploitation drifts to the surface. The entrance of the uppermost level (Santori adit) is located at 245 m a.s.l and it is connected by an inclined shaft to the intermediate level (Isabella adit, 215 m a.s.l). Both adits are excavated through serpentinized harzburgite, with a progressive increase of serpentinized dunite and gabbro lenses towards the mineralized cataclastic zone.

A vertical internal shaft connects the Isabella adit to the lowermost level of the mine, the Ribasso adit (205 m a.s.l), which emerges 700 m further north in the Pavone valley. Most of the drifts excavated in the mineralized cataclastic zone have collapsed due to the soft and soapy character of the ore body (chlorite-, serpentine-rich); hence observation is possible only in few stopes. The Isabella adit offers

the best and safest exposures of the ultramafic host rocks, crosscutting about 200 m of serpentinized harzburgite and reaching the footwall of the mineralized cataclastic zone. The intermediate part of this adit, between the entrance and the main internal shaft, displays walls and ceiling covered by white to creamy-white crusts composed mainly of carbonates (Figure 2). Something similar also occurs in the first part of the Santori adit. In particular, the whitish crusts are noticeable looking inward into the Isabella and Santori adits (Figure 2A); whereas they are not visible looking outward from the adits (Figure 2B). The Ribasso adit is flooded and observations there have been precluded. Although dripping water has been locally observed and sampled, there is not a direct spatial association between carbonate crusts and fractures discharging dripping water. Most of the walls covered by carbonates are homogeneously wet and they do not display any laminar water flow; they resemble cold surfaces covered by condensed water.

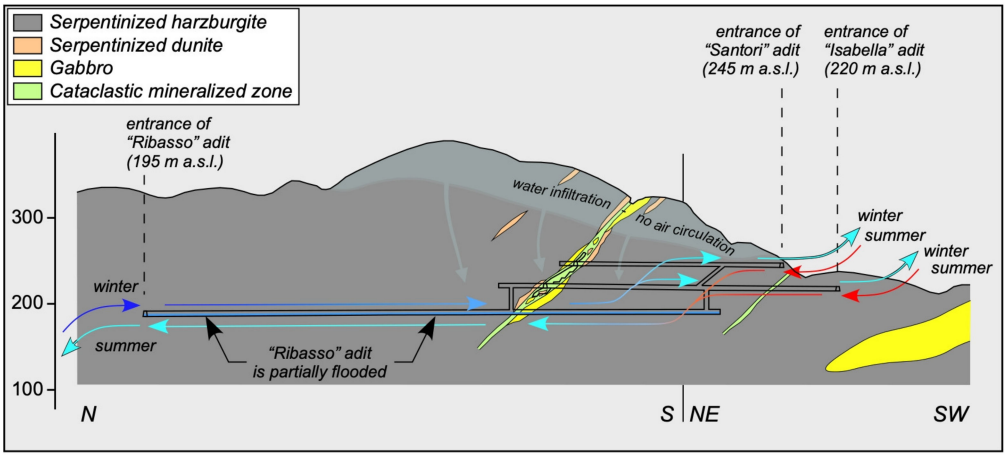

Figure 1. Cross section of the Montecastelli copper mine, showing the geological features and the overall air circulation pattern during the two main upward (winter) and downward (summer) airflow stages.

Figure 2. Isabella adit of the Montecastelli mine. (**A**) View of the adit looking inward where the white coating of hydromagnesite + kerolite and aragonite is visible and (**B**) view from the adit looking outward where the withe coating is not visible.

The hill hosting the mine is covered by a pine and oak forest and variably well-drained soils rich in organic matter. The soil allows a significant infiltration of meteoric water inside the fractured serpentinites, forming small confined aquifers which, in turn, slowly feed small perennial drippings along the underground walls, as well as small pools on the floor. The average external air temperature at Montecastelli [15] displays a typical seasonal variation with a maximum of 25 °C during August and a minimum of 6 °C during January and February (Figure 3). The maximum humidity of the external air and soil is reached during the rainy season, from October to the end of April, while the period between mid-June and late August is characterized by severe soil aridity. Air temperature and humidity inside the mine are relatively constant throughout the year (15 to 17 °C and 80% to 100%), with major fluctuations near the entrance of Isabella and Santori adits.

Owing to the configuration of the mining works, the Montecastelli mine can be classified as a dynamic underground complex [1,9–11] where ventilation is triggered by the so-called "chimney effect". The difference in elevation between the uppermost adits (Santori and Isabella) and the lowermost adit (Ribasso) triggers the air circulation, which changes seasonally. During the summer, the relatively cold air inside the mine flows out from the lowermost adit, drawing in warmer and drier air from the outside through the uppermost levels (downward airflow, Figures 1 and 3). Contrarily, during the winter, the relatively warm air inside the mine flows out from the uppermost adits (upward airflow), drawing in colder and humid air from the outside through the lowermost level (Figures 1 and 3). The direct, on-site observation of stagnant circulation during April to May and during October (weak or zero airflow), complies with the intersection between the annual cycle of external air temperature and the almost constant air temperature in the cave (Figure 3).

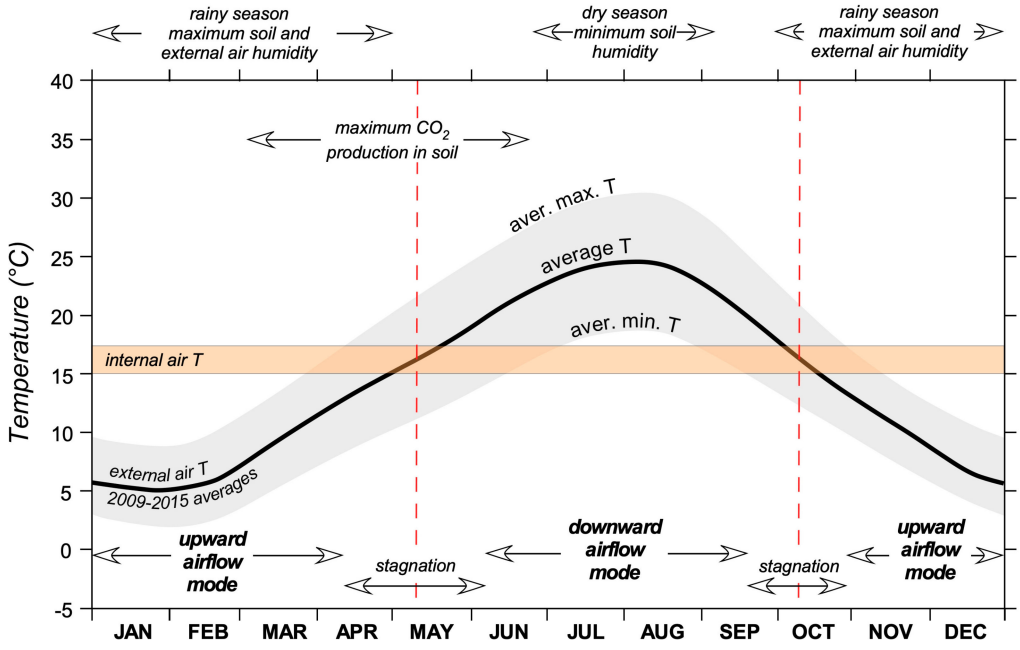

Figure 3. Diagram showing the annual cycle of external air temperature (average mean, maximum, and minimum), the air temperature in the cave, and other meteorological data with respect to the microclimatic dynamic conditions observed in the underground system. Meteorological data for Montecastelli and Castelnuovo as well as other data and information from this study are from the Tuscan Hydrologic Survey [15].

In summary, the Montecastelli underground system behaves like many multiple entrance karst undergrounds placed at midlatitudes, but with a major difference of decoupling between air and water circulation. Airflow is strictly controlled by the topography of the adits/shafts network coupled with the annual cycle of external air temperature, while the lack of large vertical fractures in the overlying

rock mass (typical of carbonate-hosted karst systems) precludes the direct arrival of CO_2-enriched air during the spring and summer time. Contrarily, meteoric water interacting with soils above the mine can dissolve an aliquot of soil CO_2, bringing it into the mine by slow infiltration through a network of tiny fractures. The lack of a massive influx of CO_2-rich air during the warm season is pivotal to the understanding of mechanisms of serpentinite carbonation along the Isabella adit.

3. Methods

Morphological and structural investigations at the microscale were carried out using field emission scanning electron microscopy (FESEM-JSM-6500F) at the National Institute of Geophysics and Volcanology (INGV, Rome, Italy). Secondary electron (SE) images, backscattered electron microscopy (BSEM) images, and X-ray element distribution maps were performed to detail wall incrustations. X-ray diffraction (XRD) patterns were obtained employing different instrumentations at the Department of Earth Science (University of Pisa, Pisa, Italy) using a Philips PW 1050/1710 with a conventional Bragg-Brentano (BB) parafocusing geometry equipped with a copper tube and a secondary graphite monochromator. The data were collected in the angular range $4° \leq 2\theta \leq 60°$, with 0.02° 2θ scan step and counting time 2 s/step operating at 40 kV and 25 mA. Mineral chemical composition was analyzed using a JXA 8200 WD/ED electron microprobe (EMP) at the INGV (Rome, Italy). The analyses were performed using 15 kV acceleration voltage, 2.6 nA beam current, and probe diameter of 5 µm with a counting time of 10 s on the peak and 5 s on the background on both sides of the peak. Estimated precision is 0.05 wt %. The detection limit is 0.01 wt % for Cl, 0.03 wt % for Al_2O_3 and Na_2O, 0.04 wt % for SiO_2, MgO and CaO, 0.05 wt % for FeOtot, MnO, NiO, 0.06 wt % for TiO_2 and Cr_2O_3, 0.09 wt % for SO_3, 0.10 wt % for K_2O.

The concentrations of Ba, Sc, V, Cr, Ni, Cu, Zn, Rb, Sr, Y, Zr, Nb, Ce, rare earth elements (REEs), Pb, Th, and U of carbonate and serpentine were determined with a sector-field, single-collector Element 2 XR ICP-MS at the University of Lausanne in laser ablation mode (LA-ICP-MS), i.e., interfaced to a NewWave UP-193 ArF excimer ablation system (ESI). Spot size varied between 75 and 100 µm with a frequency of 20 Hz and energy of 6.0 J/cm^2, using as standard NIST SRM 612. Raw data were reduced off-line using the LAMTRACE software [16]. The analytical precision is better than 8% RSD.

Seasonal mine water sampling was performed at the following two sites: (i) mine water 1, in a deeper part of the mine; (ii) mine water 2, close to the carbonate crust along the main adit. For our model we used mine water 2, because it is associated with the carbonate crust. In the field, the temperature, pH, and electrical conductivity were measured with a portable multiparameter data logger calibrated in the laboratory; total alkalinity was determined by acidimetric titration. Accuracy is 0.5% for conductivity, 0.25% for temperature, 0.05 for pH, and 0.1 meq/L for alkalinity. After the physico-chemical measurements, water samples were collected in different modes depending on the specific chemical and isotopic analyses, performed in the laboratory. Water samples for anions (SO_4^{2-} and Cl^-) and cations (Na^+ and K^+) analyses were collected without any pretreatment, while samples for Ca^{2+}, Mg^{2+}, trace elements, and silica were filtered in the field through 0.45 µm acetate-cellulose membrane filters and acidified in order to prevent precipitation. In addition, they were stored in bottles previously washed with diluted HNO_3. All water samples were stored at 4 °C prior to processing. The anions and cations were analyzed, at the Institute of Geoscience and Earth Resources of the CNR in Pisa (IGG-CNR; Italy), using a Dionex DX100 ion chromatograph and a Perkin-Elmer 3110 atomic absorption spectrometer. The analytical precision is 3% for both species. Silica determination was performed via spectrophotometric method. Trace elements were analyzed by ICP-MS at the IGG-CNR. The analytical precision is better than 2%.

Aqueous species speciation and mineral saturation indices (SI) were calculated using the geochemical speciation code PHREEQC [17] and the Base de Donnee Thermoddem_V1.10 database from the Bureau de Recherches Géologiques et Minières (BRGM Institute, Fontenay-aux-Roses, France; http://thermoddem.brgm.fr.) All the solutions were calculated based on Cl-charge balance.

4. Results

4.1. Serpentinite Substratum

Serpentinized harzburgites are composed mainly by lizardite (>95%), chlorite, magnetite, and only minor relicts of Mg-Al chromite (Figure 4a). Serpentine is present as mesh-textured matrix embedding bastite porphyroclasts with local chrysotile veins and can be intergrown with clinochlore. Primary Mg-Al chromites range in size from few microns up to ~1 mm. They show the typical lobate habit of spinels in mantle rocks and are characterized by rims of Fe-chromite. Along the Isabella adit, several cataclastic zones, plunging at a subvertical to medium angle and oriented like the main mineralized cataclastic zone, produced pervasive brecciation of serpentinized harzburgites (Figure 4b). Breccias are clast supported, with angular and subangular clasts ranging in size from submillimetric to pluri-decimetric. The matrix is constituted of fine-grained serpentine and andraditic garnet (identified by XRD). Small crystals of andradite (~2 to 3 μm in diameter) are observed both in matrix and clasts. They are anhedral and form interstitial aggregates (Figure 5).

The studied samples do not show evidence of pervasive Mg carbonation at the microscopic scale or carbonate precipitation. Coatings and crusts of hydrous Mg carbonates and Mg-clay have only been observed on the exposed rock surfaces in the mine adits.

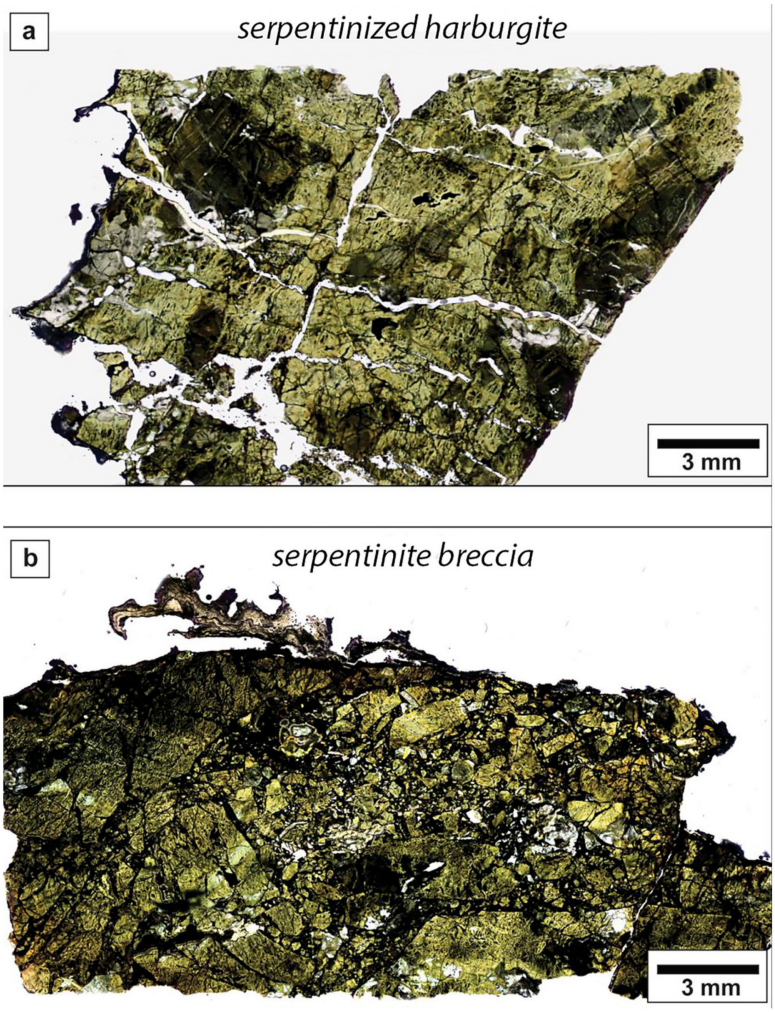

Figure 4. Thin sections of serpentinite sampled along the mine adits: (**a**) Serpentinized harzburgites and (**b**) serpentinite breccias.

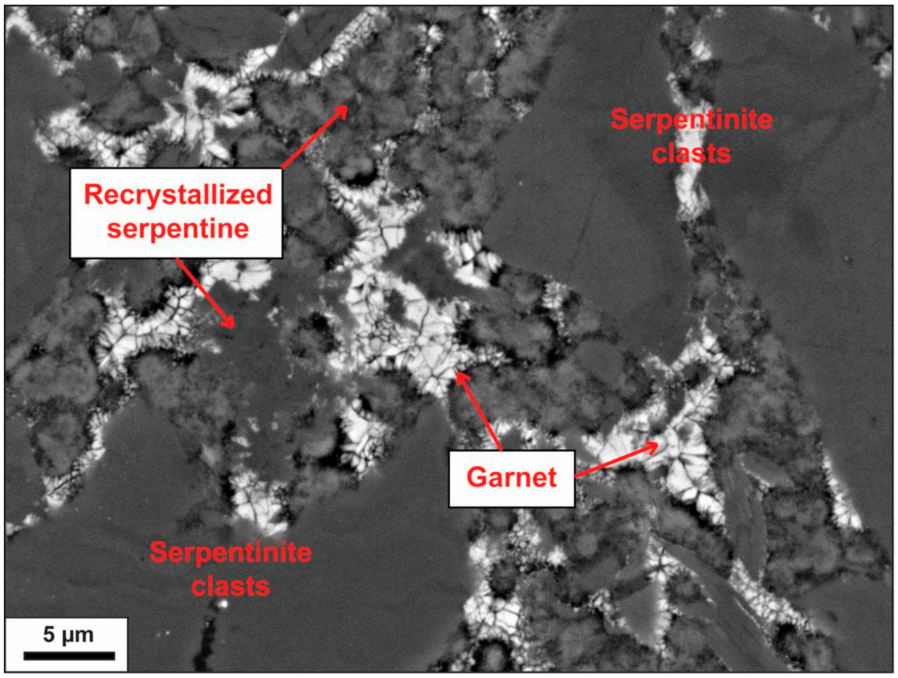

Figure 5. SEM-EDS image of interstitial andradite garnet in the matrix of serpentinite breccia.

4.2. Wall Coating

The mineral paragenesis forming the wall coating, identified by XRD and EMP analyses, is represented by hydromagnesite, with minor aragonite and a Mg-rich clay silicate (Figure S1, Table S1 and S2 in Supplementary Materials, SM). Macroscopically, hydromagnesite occurs mostly as coatings, crusts, and spherules lining the rock surfaces and tiny fractures propagating for a few millimeters into the serpentinite walls (Figure 6). Coatings, crusts, and spherules can have a large areal extension but with a limited thickness, up to few millimeters.

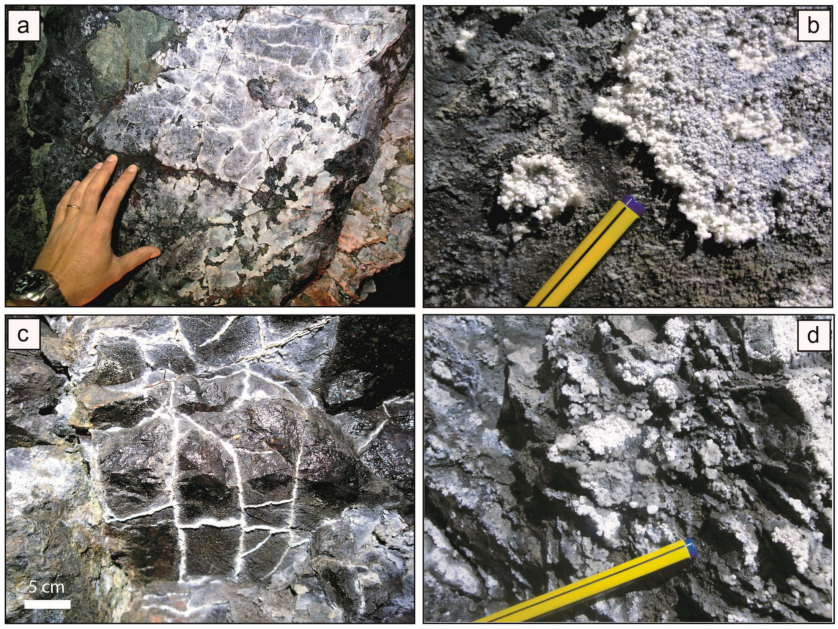

Figure 6. Examples of carbonate coatings: (**a**) Hydromagnesite ± kerolite coating (first precipitation), (**b**) hydromagnesite rosettes (second precipitation), (**c**) early precipitation of hydromagnesite along the rock fractures, and (**d**) preferential precipitation of hydromagnesite on the surfaces facing outwards of the mine adit.

At the microscale, two episodes of hydromagnesite precipitation are recognized (Figures 7 and 8). The first precipitation is characterized by hydromagnesite layers alternated with Mg-rich clays layers (with thicknesses ranging from 100 µm to <5 µm; Figure 8). In particular, the Mg-clays layers, generally deposited in the late stage, and showed an irregular and wavy texture with the presence of shrinkage cracks (<5 µm in width). The second episode of precipitation formed an aggregate of hydromagnesite rosettes, each made by fibrous-radiating acicular crystals (with size ranging from ~1 to >8 µm). This generation forms an external coating, distinguished from the early precipitation by a strong increase in porosity (Figure 8). Minor amounts of anhedral aragonite (with size ranging from ~500 µm to a few micrometers) have been observed in association with both hydromagnesite µm (Figure 8). We found partially dissolved serpentine fines, with a size variable from 5 to 200 microns, forming a layer between the serpentinite and the crusts (Figure 8b–f). This powdered serpentine was most likely produced during the mine excavation.

The chemical composition of Mg-clays (Table S2) can be attributed to either stevensite or a hydrated and highly disordered variety of talc-like phase, named "kerolite" $Mg_3Si_4O_{10}(OH)_2 \cdot nH_2O$ [18–20]. Kerolite-like minerals are usually associated with carbonates derived from alteration of ultramafic rocks at high pH [20], whereas stevensite is more common in low pH environments. In addition, the XRD data points to the presence of "kerolite" rather than stevensite (Figure S1). "Kerolite" has previously been found mixed with poorly crystalline serpentine, both in natural settings and in experimental reaction products [15]. The term "deweylite" has been used to describe intimate mixtures of a fine-grained, highly disordered, kerolite-like mineral and a disordered serpentine mineral, typically chrysotile, in varying proportions. This is in agreement with our variable chemical analyses, indicating an excess of Mg and a deficiency of Si, probably because of the presence of serpentine and (or) disordered kerolite (Table S2).

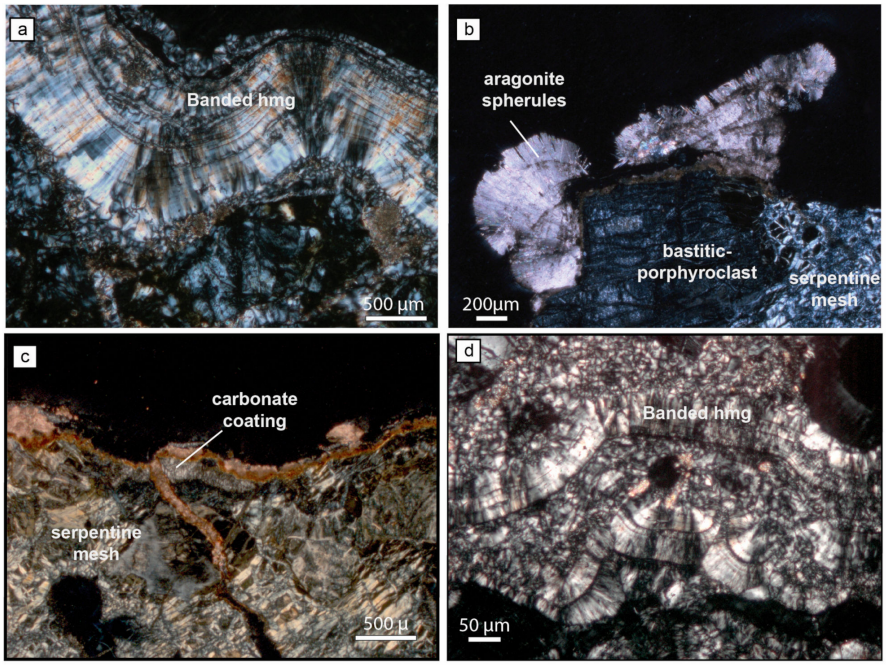

Figure 7. Microphotographs of various carbonate occurrences showing: (**a**) Banded hydromagnesite and kerolite; (**b**) aragonite spherules growth onto carbonate coating + bastite porphyroclasts; (**c**) carbonate coating composed of hydromagnesite, kerolite, and late aragonite; and (**d**) overgrowths of banded hydromagnesite.

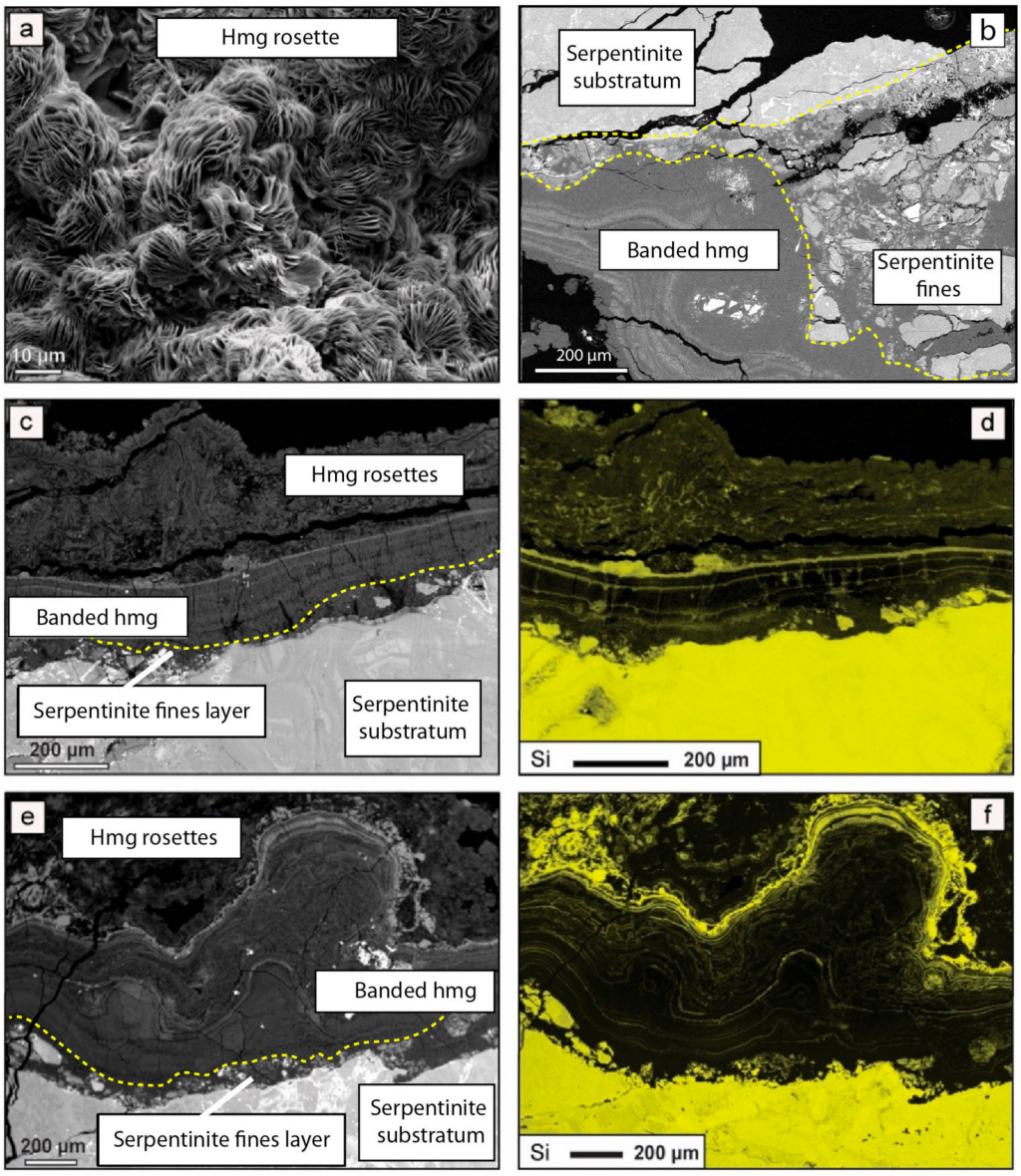

Figure 8. SEM images and X-ray element distribution maps of wall incrustations: (**a**) Secondary electron (SE) image showing intergrowth of lenticular crystals of hydromagnesite on the outer layer of the crusts; (**b**) backscattered electron microscopy (BSEM) image showing the serpentine fines embedded into hydromagnesite ± kerolite. Kerolite layers are distinguishable from hydromagnesite layers because they appear light grey in color in the BSEM images; (**c**–**f**) BSEM images (**c** and **e**) and X-ray element distribution maps for Si (**d** and **f**) showing the following: (i) serpentinite substratum, (ii) serpentinite fines at the external surface of the rock, (iii) hydromagnesite and kerolite layered crust, and (iv) late hydromagnesite rosettes. The yellow color in Figure 8d,f highlights the presence of kerolite layers and serpentinite fines on the wall surface.

4.3. Trace Element Composition of Mineral Phases

Trace element composition of serpentine and hydromagnesite analyzed by LA-ICP-MS is reported in Tables 1 and 2. Serpentine minerals have high Cr and Ni content, up to ~2600 ppm and ~1400 ppm, respectively, relatively high content of V and Cu, and detectable content of Pb, U, Th, Y, Rb, Sr, Zr, and Nb. REE serpentine patterns span over a relatively small range of contents; from ~0.1 to more ~1 times those of the chondritic values, with LREE depleted patterns and a positive Eu anomaly (Figure 9).

Table 1. Trace element composition (ppm) of serpentine determined by LA-ICP-MS.

Sample Type	MA22B	MA22D	MA22F	MA22H	MA22L	MA29B	MA29D	MA29F	MA29H	MA29L
	serp	serp	serp	serp	serp	serp	serp	serp	serp	serp
V	10	10	6	7	4	26	3	54	84	41
Cr	77	112	54	52	45	477	21	1719	3149	949
Ni	1394	1356	1363	1221	1249	1431	1391	791	719	1330
Cu	8	8	10	6	6	7	5	7	24	6
Rb	0.060	0.047	0.035	0.043	0.040	0.039	0.017	0.042	0.058	0.048
Sr	1	1	1	1	1	1	1	1	1	2
Y	0.340	1.359	0.684	0.857	0.510	1.055	0.412	0.537	1.522	1.232
Zr	0.050	0.181	0.070	0.114	0.060	0.252	0.065	0.285	0.995	0.321
Nb	0.001	0.001	0.001	0.003	0.001	0.002	0.002	0.002	0.003	0.002
La	0.020	0.028	0.028	0.042	0.020	0.034	0.025	0.023	0.063	0.042
Ce	0.060	0.111	0.097	0.143	0.060	0.113	0.078	0.067	0.154	0.144
Pr	0.010	0.017	0.016	0.023	0.010	0.015	0.010	0.010	0.022	0.017
Nd	0.060	0.116	0.094	0.133	0.063	0.088	0.053	0.062	0.136	0.100
Sm	0.020	0.049	0.031	0.042	0.022	0.031	0.017	0.023	0.050	0.036
Eu	0.020	0.036	0.032	0.039	0.021	0.036	0.022	0.021	0.037	0.042
Gd	0.030	0.094	0.050	0.067	0.040	0.059	0.030	0.042	0.109	0.072
Tb	0.004	0.019	0.009	0.013	0.007	0.011	0.005	0.008	0.022	0.014
Dy	0.030	0.170	0.073	0.103	0.054	0.099	0.043	0.065	0.196	0.126
Ho	0.010	0.044	0.019	0.026	0.013	0.027	0.010	0.016	0.052	0.034
Er	0.030	0.148	0.065	0.087	0.045	0.095	0.033	0.056	0.185	0.118
Tm	0.005	0.024	0.011	0.014	0.007	0.015	0.005	0.010	0.032	0.020
Yb	0.030	0.173	0.082	0.101	0.057	0.113	0.040	0.072	0.256	0.142
Lu	0.006	0.027	0.014	0.016	0.010	0.019	0.007	0.013	0.043	0.024
Pb	0.018	0.036	0.011	0.025	0.091	0.021	0.017	0.008	0.035	0.024
Th	0.001	0.001	0.001	0.002	0.001	0.002	0.002	0.001	0.001	0.002
U	0.003	0.005	0.003	0.003	0.004	0.004	0.004	0.003	0.003	0.006

serp = serpentine.

Table 2. Trace element composition (ppm) of hydromagnesite and aragonite determined by LA-ICP-MS.

Sample Type	MA22A	MA22C	MA22E	MA22G	MA22I	MA29A	MA29C	MA29E	MA29G	MA29A	MA29L
	Hmg	Hmg	Hmg	Hmg	Hmg	Hmg	Hmg	Hmg	Hmg	Ar	Ar
Sc	0.033	0.160	0.032	0.310	0.022	0.564	0.210	0.117	0.086	0.188	0.253
V	2	4	2	3	2	5	4	2	2	1	1.1
C	41	16	18	44	11	23	13	10	18	15	12
Ni	4	1	2	15	1	5	11	1	1	5	11
Zn	1.184	1.500	1.020	1.460	3.800	0.893	0.680	2.790	0.357	0.645	1.823
Rb	0.131	0.150	0.120	0.130	0.090	0.199	0.060	0.050	0.028	0.066	0.113
Sr	3	1	1	5	1	28	16	2	1	836	1480
Y	0.023	0.008	0.010	0.030	0.004	0.030	0.030	0.008	0.008	0.060	0.16
Zr	0.116	0.071	0.042	0.120	0.035	0.208	0.070	0.026	0.037	0.137	0.14
Nb	0.004	0.002	0.002	0.005	0.002	0.008	0.004	0.002	0.002	0.005	0.006
Ba	0.394	0.137	0.100	0.439	0.100	0.596	0.540	0.129	0.092	5.070	4.91
La	0.013	0.007	0.003	0.018	0.003	0.029	0.020	0.004	0.005	0.033	0.04
Ce	0.024	0.017	0.004	0.040	0.007	0.072	0.030	0.007	0.010	0.058	0.06
Pr	0.003	0.003	0.002	0.010	0.001	0.010	0.007	0.001	0.001	0.009	0.014
Nd	0.012	0.010	0.006	0.030	0.003	0.030	0.027	0.003	0.005	0.028	0.075
Sm	0.004	0.003	0.001	0.006	0.002	0.008	0.011	0.001	0.002	0.009	0.017
Eu	0.001	0.001	<d.l.	0.002	0.001	0.003	0.003	0.001	0.001	0.002	0.008
Gd	0.006	0.007	0.005	0.009	<d.l.	0.011	0.014	0.008	< d.l.	0.008	0.021
Tb	0.001	0.001	0.001	0.001	0.000	0.001	0.001	-	0.000	0.002	0.003
D	0.003	0.003	0.003	0.007	0.001	0.006	0.007	0.002	0.002	0.007	0.014
Ho	0.001	0.001	0.001	0.001	0.000	0.002	0.001	0.001	0.000	0.002	0.004
Er	0.003	0.002	0.002	0.006	0.001	0.005	0.004	0.001	0.001	0.004	0.011
Tm	0.000	0.001	0.000	0.001	0.000	0.001	0.001	0.000	0.000	0.001	0.001
Yb	0.003	0.003	0.003	0.007	0.001	0.005	0.005	0.003	0.002	0.004	0.004
Lu	0.000	-	0.001	0.001	-	0.001	0.001	0.000	-	-	0.001
Pb	0.345	0.276	0.199	0.365	0.277	0.538	0.603	0.332	0.248	0.322	0.385
Th	0.004	0.003	0.001	0.005	0.001	0.009	0.003	0.001	0.002	0.005	0.005
U	0.007	0.003	0.003	0.006	0.002	0.010	0.003	0.007	0.003	0.008	0.007

d.l. = detection limit; - = not determined; Hmg = Hydromagnesite; Ar = aragonite.

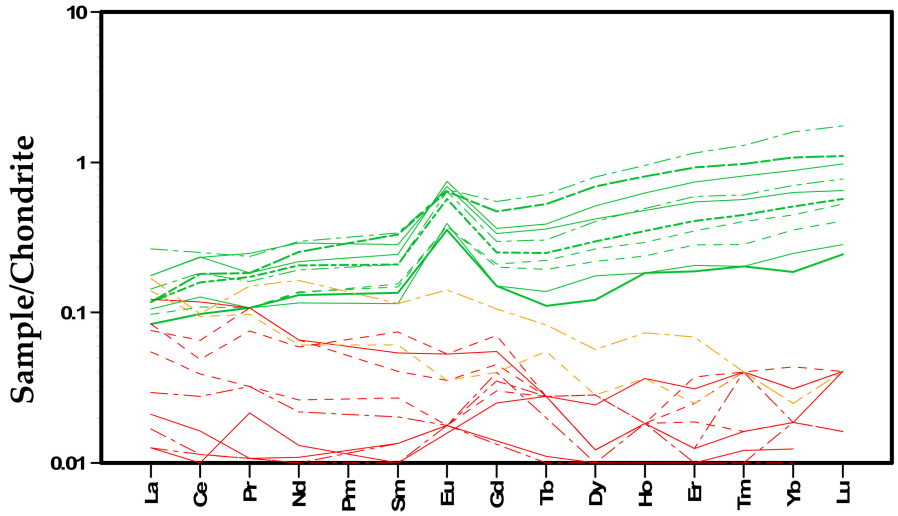

Figure 9. Trace element composition normalized to chondrite of hydromagnesite (red lines), serpentine (green lines), and aragonite (yellow lines).

Hydromagnesite shows up to 45 ppm of Cr, significant amounts of Ni, Zn, Sr, V, Ba, and Pb, and detectable REE, U, Th, Y. Hydromagnesite displays a depleted and scattered REE pattern with slightly enriched LREE ($La_N/Yb_{N(av)}$ = 1.86).

Hydromagnesite trace elements indicate that the fluid responsible for its deposition is a fluid that interacted with serpentinite host rocks. The low-temperature weathering of serpentinites produces spring waters containing a significant content of Cr, as well as Ni, Co, and Mn [1,9,21].

4.4. Chemical Composition of Mine Waters

Waters emerging from the mine walls and ceiling have a mean temperature of ~17.5 °C and a pH of ~8.4 throughout the year and can be classified as bicarbonate-magnesium type waters, because of their high Mg^{2+} and HCO_3^- concentrations, ranging from ~90 to 132 mg/L and ~7.7 to 10.0 mg/L, respectively (Table 3 and Figure 10) and show low Ca/Mg molar ratio (<0.04, Figure 10a). In the Mg-SiO_2-HCO_3 triangular diagram (Figure 10b), a mixing line between an aqueous phase in equilibrium with carbonates and Mg-rich silicates is reported. Mine waters fall to the left side of the line, indicating that such waters are in equilibrium with hydrous Mg-carbonates. Mine waters show low concentrations of trace elements, locally below detection limits, as reported also in other emerging waters in Tuscany [11]. Significant amounts of Cr (~24 ppb), Sr (~20 ppb), Ba (~85 ppb), Fe (~25 ppb) and Zn (~7 ppb) have been detected (Table 3). Other trace elements (Ni, Mn, B, V, Al, Th, and U) have very low concentration between <0.01 and up to 5 ppb. The pCO_2 and saturation indices (SI) of the relevant phases (hydromagnesite and aragonite) were calculated using the chemistry of mine waters using the PHREEQC code. Mine waters 2, collected near the carbonate crusts, show log pCO_2 varying from –3.06 to –3.04 and they are undersaturated with respect to hydromagnesite (SI_{hmg} ~–4.81) and saturated with respect to aragonite (SI_{arag} –0.03).

Table 3. Chemical composition of mine waters.

Sample		**Mine Water 1**	**Mine Water 1**	**Mine Water 1**	**Mine Water 1**	**Mine Water 1**	**Mine Water 1**	**Mine Water 1**	**Mine Water 2**	**Mine Water 2**
Date		**08/06/2011**	**29/05/2013**	**17/07/2014**	**11/10/2014**	**03/12/2014**	**18/02/2015**	**02/05/2015**	**03/12/2014**	**18/02/2014**
T	°C	18.2	17.4	17.5	17.9	17.4	17.2	17.7	17.0	17.4
pH		8.2	8.3	8.3	8.2	8.4	8.6	8.7	8.4	8.4
Alk	meq/L	9.0	8.5	10.0	9.4	9.6	9.3	9.4	4.7	4.5
Cl^-	mg/L	22.3	23.6	23.5	20.8	23.9	16.7	32.3	7.9	7.7
SO_4^{2-}	mg/L	25.5	29.2	27.1	28.8	29.4	26.1	24.7	-	-
Na^+	mg/L	10.5	10.9	11.7	11.4	12.3	10.2	15.2	-	-
K^+	mg/L	0.4	0.1	0.1	0.1	0.2	0.2	0.1	-	-
Ca^{2+}	mg/L	6.4	8.7	8.6	8.0	7.2	8.0	5.4	8.5	8.7
Mg^{2+}	mg/L	116.0	114.0	131.6	114.9	115.9	116.7	113.2	89.8	90.7
Si as SiO_2	mg/L	-	29.1	32.4	30.3	28.2	28.9	13.6	29.8	30.0
Cr	µg/L	25.0	22.7	27.0	24.0	22.7	-	22.5	-	-
Sr	µg/L	25.0	18	19	19	19	-	18	-	-
Ba	µg/L	-	-	105.0	37.0	94.0	-	103.0	-	-
B	µg/L	-	-	-	-	4.0	-	4.0	-	-
Fe	µg/L	-	-	-	-	33.3	-	17.2	-	-
Mn	µg/L	-	-	-	-	1.5	-	1.8	-	-
Ni	µg/L	-	-	-	-	5.7	-	2.2	-	-
Pb	µg/L	-	-	-	-	0.1	-	0.7	-	-
Cu	µg/L	-	-	-	-	0.4	-	1.0	-	-
Zn	µg/L	-	-	-	-	46.0	-	27.0	-	-
V	µg/L	-	-	-	-	1.3	-	1.4	-	-
Al	µg/L	-	-	-	-	<1	-	<1	-	-
Th	µg/L	-	-	-	-	<0.01	-	<0.01	-	-
U	µg/L	-	-	-	-	<0.01	-	<0.01	-	-

- = not determined.

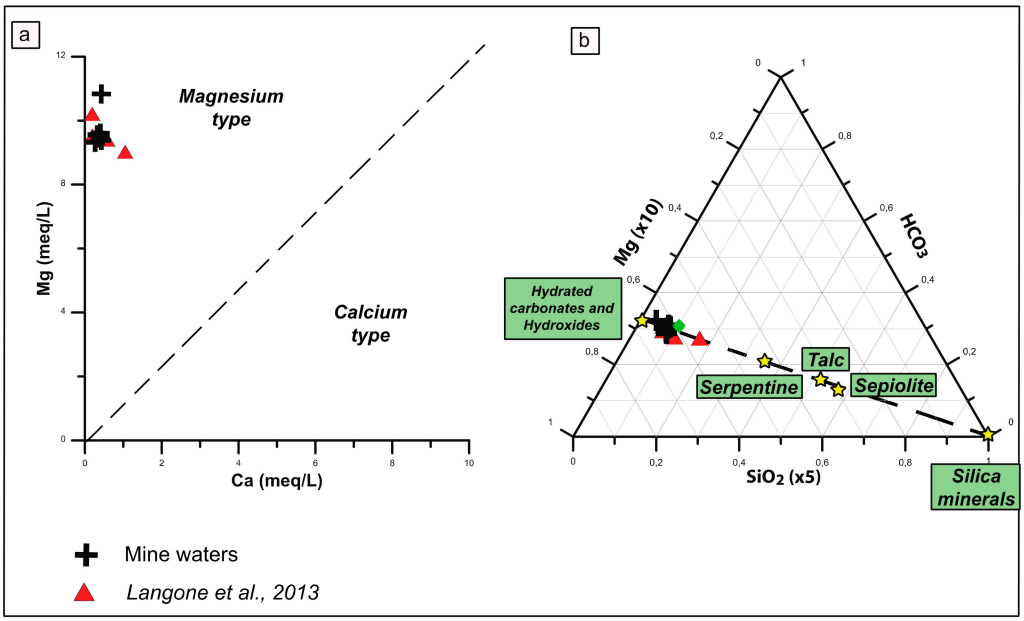

Figure 10. Chemistry of mine waters. (**a**) Mg vs. Ca plot computed from concentrations in meq/L and (**b**) Mg-SiO_2-HCO_3 triangular plot, computed from concentrations in mg/L. Red triangular points represent from another mine excavated in serpentinites from Southern Tuscany (Querceto, [11]) and stairs represent the expected compositions of aqueous phases controlled by CO_2-driven dissolution of Mg-bearing solid phases (i.e., sepiolite, talc, serpentine, and hydrated carbonates).

5. Discussion

Underground environments, such as mine adits and natural caves, have peculiar characteristics, such as an almost constant temperature throughout the year, high humidity, and seasonal variation of the direction of ventilation [22]. Cyclical variations of these parameters can enhance CO_2 degassing, as well as water evaporation and condensation that can trigger carbonate precipitation [22–24]. Even though the formation of underground carbonate concretions in natural caves has been well understood, the formation of various types of concretions in mining underground works, especially with ultramafic substratum, is still lacking a thorough investigation. The study of this latter type of concretion in an ultramafic underground environment, such as the Montecastelli Cu mine, can give the opportunity to explore the peculiar conditions at which CO_2-rich water spontaneously react with serpentinite rocks.

5.1. PHREEQC Models

Petrographic and XRD data shows that the wall coating paragenesis in the Montecastelli mine is composed of hydromagnesite, kerolite, and aragonite precipitated. In order to understand whether the coating precipitated directly from dripping waters we performed geochemical modeling with PHREEQC using as starting fluid waters emerging from the fractures in the mine wall close to the carbonate crusts (mine water 2). Our model indicates that the CO_2-rich dripping water (log pCO_2 = −3.05) moves towards equilibrium with the pCO_2 of the mine atmosphere (log pCO_2 = −3.40 corresponding to ~418 ppmv) measured along the mine adits (Table 4). After the pCO_2 of the dripping water equilibrates with that of the mine, it becomes saturated with aragonite (SI_{arag} = 0.25) and undersaturated in hydromagnesite (SI_{hmg} = −3.09).

Aragonite supersaturation (SI > 0.45) is reached through evaporation (more than 20%, Table 5), allowing its precipitation. Dripping water becomes supersaturated in hydromagnesite (SI = 0.46) with higher incremental evaporation (more than 55%), letting hydromagnesite precipitation after aragonite. Therefore, the observed mineral paragenesis of the wall coating, where hydromagnesite is the first phase to precipitate, cannot be generated directly from dripping waters.

Table 4. CO_2 measured along the mine adits.

Sample	Date	Site	CO_2 (ppmv)	St.dev.	log pCO_2
1	18/02/2015	adit near hysromagnesite crust	430	17	−3.37
2	18/02/2015	adit near the exit of the mine	418	11	−3.38
3	18/02/2015	adit in the upper part	399	16	−3.40
4	18/02/2015	adit in the middle part	377	1	−3.42
5	18/02/2015	Mine outside	367	2	−3.44
1	02/05/2015	adit near hysromagnesite crust	430	3	−3.37
2	02/05/2015	adit near the exit of the mine	436	1	−3.38
3	02/05/2015	adit in the upper part	415	4	−3.37
4	02/05/2015	adit in the middle part	435	4	−3.36
5	02/05/2015	Mine outside	412	3	−3.39

St.dev. = Standard deviation.

Table 5. Saturation indeces of hydromagnesite and aragonite, pH and Mg/Ca molar ratio of dripping and condensed waters computed in PHREEQC.

Evaporation %	10	20	30	40	50	55	80	85
			Dripping water					
log pCO_2	−3.4	−3.4	−3.4	−3.4	−3.4	−3.4	−3.4	−3.4
pH	8.75	8.78	8.83	8.86	8.9	8.93	8.82	8.78
SI_{hmg}	−2.56	−1.98	−1.49	−0.8	−0.01	0.46	0	0
Si_{ar}	0.34	0.45	0.25	0.25	0.25	0.25	0.25	0.25
Mg/Ca (molality)	17.19	17.19	34.46	46.95	67.08	82.08	68.99	69.63
			Condensed water					
log pCO_2	−3.4	−3.4	−3.4	−3.4	−3.4	−3.4	−3.4	−3.4
pH	8.42	8.45	8.52	8.58	8.65	8.69	8.96	9.05
SI_{hmg}	−8.4	−7.72	−6.95	−6.08	−5.07	−4.5	−0.46	0.81

Previously, it has been shown that the formation of Mg-carbonate wall coating in underground mines, excavated in ultramafic lithologies, can also occur through direct precipitation from dripping waters [2]. However, the dripping waters in this case [2] interacted mainly with brucite, and therefore became enriched in Mg^{2+} but not in Ca^{2+} (0.36 to 1.02 mg/L) or Si^{4+} (0.0 to 9.3 mg/L) which prevented the precipitation of aragonite and kerolite. At Montecastelli, instead, dripping waters interacted prevalently with serpentinized harzburgite (Figure 4 and Table 3), and in a minor amount with gabbro lenses which outcrop in the area, therefore, they became relatively enriched not only in Mg^{2+} but also in Ca^{2+} (5.4 to 8.7 mg/L) and Si (13.6 to 32.4 mg/L).

An alternative model has been elaborated considering the water film on the adits' walls that could have been derived from evaporation of dripping and pooled waters, as well as by ingress of humid air from outside. The chemical composition of this "condensed" water is assumed corresponding to a distilled water ($Mg^{2+} \leq 0.01$, $Si^{4+} \leq 0.01$, and $Ca^{2+} \leq 0.01$ in mg/L) in equilibrium with pCO_2 of the air in the mine. We hypothesized that the condensed water became enriched in ions after the dissolution of serpentine fines and the equilibration with pCO_2 of the air. The mineral paragenesis, dissolution reactions, and equilibrium constants (log k) at 25 °C and 1.013 bar are listed in Table S3. Our model shows that the condensed water on the mine walls after interacting with the serpentine fines would have a content of Mg^{2+} ~22 mg/L, SiO_2 ~36.2 mg/L, and HCO_3^- ~105 mg/L, with a pH of 8.38. This fluid is undersaturated in hydromagnesite (SI_{hmg} ~−9.02). Hydromagnesite supersaturation can be slowly reached by evaporation (up to 85%, SI_{hmg} ~0.81), whereas aragonite cannot precipitate due to the absence of Ca^{2+}. Therefore, this process can explain the observed wall coating paragenesis, where hydromagnesite is the first mineral to precipitate.

5.2. Interaction between Condensed Water and Mine Wall Serpentinite

Even though the dissolution of serpentine could provide the cations required for the precipitation of the wall coating paragenesis, serpentine is known to have low solubility at low-temperature conditions [25–28]. This is confirmed by our microscopic investigations showing that there is no evidence for the dissolution of serpentine in the substratum of the carbonate crusts (Figure 8). However, we have observed a discontinuous layer of serpentine fines at the interface between mine walls and carbonate crusts in all the studied samples. The presence of a layer of serpentine fines on the mine wall is most likely a consequence of the shafts and adits excavation. Underground excavation in the early half of the XIX century was done using dry jack hammers which generated a high amount of powder from the serpentine rocks which coated the adit walls and was progressively glued by condensing waters.

It is known that the dissolution rate, and reactivity, of serpentine with CO_2 is strongly enhanced by the increase of the reactive surface area [27,28]. Therefore, serpentine fines represent an efficient reagent from which CO_2-rich condensed water could have progressively stripped Mg and Si required for the formation of the wall coating paragenesis. As observed by FEG-SEM, both the serpentinite fine layer and the new hydromagnesite crusts are highly porous (Figures 7 and 8). They could play as a capillary-drying system where the condensed water infiltrates through the porosity, mostly uptaking Mg and Si along the surfaces of the serpentine particles and crystallizing new minerals (hydromagnesite or kerolite) on the outer surface of the fine layer and the previously crystallized crusts.

Such an interpretive model can be further discussed considering the boundary layer effect in the water film forming on the external surface of the crust. Here, the hydromagnesite precipitation induces a Mg-depleted boundary layer. The higher Si/Mg ratio could temporarily stabilize the precipitation of a kerolite band. The interplay between dissolution/crystallization and diffusion kinetics could generate the complex hydromagnesite-kerolite banding. Condensed water could also propagate into small fractures from the rock surface dissolving chrysotile. In this case, the chemistry of the resulting fluids would be comparable with that resulting from the interaction with the serpentine fines. However, considering the aerial extension of these veins, the overall effect contribution to the carbonation process is expected to be limited as compared with the fines layer. Therefore, we consider the spontaneous carbonation in the Montecastelli mine mainly driven by the presence of the serpentinite fines.

5.3. Seasonally Driven Deposition of the Carbonate Crusts

Geochemical modeling showed that precipitation of wall carbonates is driven by evaporation of modified condensed water on the adit walls. The most peculiar feature of the crusts is their distribution along both sides of the adit walls. Adit walls have an irregular surface with peaks and throughs of variable sizes resulting from their excavation. These irregularities produce a continuous alternation of rock surfaces, which are facing inward and outward from the adit entrance. The carbonate-kerolite crusts are present only on the outward looking faces (Figure 6d).

Considering that the mine environment has a stable temperature and humidity, such an asymmetric distribution needs to be explained by a selective depositional process. Seasonal changes of air circulation inside the mine can explain this observation because they can trigger the preferential evaporation of condensed water on the outward looking surfaces. As described before, during summer the relatively colder and heavier air inside the mine flows out from the lowermost level, drawing the hot and dry air from outside into the upper adits. Contrarily during winter, the relatively warm and light air inside the mine flows out from the upper levels, while drawing in colder and humid air from the outside through the lowermost adit. In the latter case, incoming air becomes progressively more humid flowing through the flooded lowermost adit. Therefore, the optimal condition for selective evaporation of water condensed on the outward looking surfaces of the upper adits is attained during summer because the air flow is dry (Figure 1). Instead, winter air circulation is dominated by humid air, which cannot promote evaporation of condensed water (Figure 1).

Typical carbonate-hosted caves at similar midlatitudes behave differently. Seasonal cyclicity in temperature and air density, coupled with enhanced CO_2 production in soils during the warm season, is commonly responsible for the relevant summer CO_2 buildup in cave air and the inhibition of calcite precipitation by elevated CO_2 levels in the cave waters. Maximum speleothem growth occurs during the cold season when the airflow inversion introduces CO_2-poor air in the cave and the CO_2 level in cave water is strongly reduced [22–24] The reverse behavior at the Montecastelli mine is easily understood considering the different precipitation process (evaporation-condensation-evaporation) and the peculiar topographic and geologic characters of this artificial underground system that prevent extreme CO_2 buildup during the warm season.

The interaction between condensed water and serpentine minerals on the wall surface can be summarized as by Equation (1), that is compatible with the precipitation of alternating bands of hydromagnesite and kerolite:

$$6Mg_3Si_2O_5(OH)_2 \text{ (Serpentine)} + 4HCO^-_3 + 5H_2O \rightarrow 3Mg_3Si_4O_{10}(OH)_2{\cdot}H_2O \text{ (Kerolite)} + Mg_5(CO_3)_4(OH)_2{\cdot}4H_2O \text{ (hydromagnesite)} + 4Mg^{2+} + 2(OH)_2 \quad (1)$$

The presence of small amounts of aragonite can be related both to the partial dissolution of Ca-rich minerals, present in very minor amount in the serpentinites. Kerolite precipitation is thought to be promoted by low temperature, high pH, and high silica and magnesium activity [20]. Saturation of amorphous silica at high pH (>8.2) has also been proposed as a key condition for the precipitation of Mg-silicates [18–20]. Condensed waters in the Montecastelli mine has high pH (~8.9), high Mg content (>70 mg/L), and high dissolved silica activity, which are required for the precipitation of kerolite, and thus further supporting the genetic process.

6. Conclusions

In this study, we have reported a new occurrence of spontaneous CO_2 sequestration through the formation of hydromagnesite and kerolite on serpentine mine walls in the Montecastelli Cu mine located in Southern Tuscany, Italy. The formation of hydromagnesite and kerolite is triggered by the interaction between condensed water with serpentinite fines accumulated on the walls of the adits during excavation. The large surface area of the fines strongly increases the reactivity of serpentine and allows its dissolution at low temperature. This provides the required elements for the precipitation of the wall coating assemblage. The precipitation takes place due to the selective evaporation of water on upwind rock surfaces exposed to the downward circulation during summer. The peculiar features of this occurrence include the following: (i) the instauration of unusual microclimatic condition in this artificial underground system and (ii) the spontaneous carbonation of serpentine at low temperature. The latter has usually not been observed in ultramafic outcrops exposed on the Earth's surface, where, instead, hydromagnesite predominantly forms through the dissolution of the more reactive brucite.

This study shows that serpentine carbonation at low temperature is possible and it could be reproduced in ex situ applications by using fine-grained serpentine powder and a cyclical process of condensation and evaporation steps. The efficiency of this process can be tested and implemented through laboratory experiments and could have a significant impact on the applicability of CO_2 mineral sequestration because it does not require pretreatment of serpentine or high temperature during the reaction, thus, potentially reducing the costs.

Further study of the peculiar conditions of underground environments hosted in Mg-rich lithologies, such as that of the Montecastelli Cu mine, can lead to a better understanding of the physical and chemical conditions necessary to enhance serpentine carbonation at low temperature, and thus implementation of new strategies for engineered CO_2.

Supplementary Materials: The following are available online at http://www.mdpi.com/2075-163X/10/1/1/s1, Table S1: Microprobe analyses (wt %) of Montecastelli mine hydromagnesites, Table S2: Microprobe analyses (wt %) of "deweylite"—a variable mixture of kerolite and serpentine—identified in the wall coating, Table S3: Dissolution reactions and thermodynamic equilibrium constants for considered minerals at 25 °C and 1.013 bar;

and Figure S1: XRD of the coating paragenesis showing the characteristic peaks of hydromagnesite (red bars), aragonite (green bars), and clay minerals (* symbol). As it can be seen in the inserted closeup, the presence of kerolite in the specimen is demonstrated by the small angular shift and by the definitely larger FWHM of the diffraction peak at near 9.4 Å, where diffractions of kerolite and hydromagnesite overlap. In fact, the other diffraction peak at higher angle, due to the diffraction of hydromagnesite only show a definitely smaller FWHM.

Author Contributions: For research articles with several authors, a short paragraph specifying their individual contributions must be provided. The following statements should be used "conceptualization, C.B. and A.D.; methodology, C.B., I.B., L.B., N.P., A.U. and A.D.; software, F.B., I.B., L.B. and A.U.; validation, C.B., I.B., N.P., A.U. and A.D.; formal analysis, C.B., F.B., I.B., N.P., A.U.; investigation, C.B., I.B., F.B. and A.D.; resources, C.B., L.B., N.P. and G.Z.; data curation, F.B., I.B., A.R.; writing—original draft preparation, C.B., F.B., A.R. and A.D.; writing—review and editing, C.B., I.B., A.R., N.P., A.U. and A.D.; visualization, C.B., F.B., I.B., A.R., N.P. and A.D.; supervision, C.B. and A.D.; project administration, C.B.; funding acquisition, C.B., F.B. and G.Z. All authors have read and agree to the published version of the manuscript. All authors have read and agreed to the published version of the manuscript.

Funding: This research was partially funded by European Horizon 2020 GECO project (https://geco-h2020.eu), grant number 818169. The F.B. was supported by the Pegaso PhD project (Tuscan Region, Italy). C.B. was partially supported by a SNSF grant (Swiss National Science Foundation; i.e., International Short Visits, grant number IZK0Z2_158572.) and by Fondation Herbette (Universitè de Lausanne) grant for her work at the University of Lausanne.

Acknowledgments: C.B. and co-authors thank Gianluca Giorgi, the owner of the Montecastelli Mine (https://sites.google.com/site/minieradelpavone/) that recently passed away. Gianluca allowed us to study the mine geology and helped us to sample fluids, rocks, and coating. C.B. and F.B. thank Othmar Müntener for his availability and scientific and analytical support during their stay at the University of Lausanne. The authors thank two anonymous reviewers for their critical review of an earlier version of the manuscript and the Guest Editor Giovanni Ruggieri for supporting our proposal and assisting us with this special issue.

Conflicts of Interest: The authors declare no conflict of interest.

References

1. Boschi, C.; Dini, A.; Baneschi, I.; Bedini, F.; Perchiazzi, N.; Cavallo, A. Brucite-driven CO_2 uptake in serpentinized dunites (Ligurian Ophiolites, Montecastelli, Tuscany). *Lithos* **2017**, *288*, 264–281. [CrossRef]
2. Beinlich, A.; Austrheim, H. In situ sequestration of atmospheric CO_2 at low temperature and surface cracking of serpentinized peridotite in mine shafts. *Chem. Geol.* **2012**, *332*, 32–44. [CrossRef]
3. Power, I.M.; Wilson, S.A.; Thom, J.M.; Dipple, G.M.; Gabites, J.E.; Southam, G. The hydromagnesite playas of Atlin, British Columbia, Canada: A biogeochemical model for CO_2 sequestration. *Chem. Geol.* **2009**, *260*, 286–300. [CrossRef]
4. Teir, S.; Eloneva, S.; Fogelholm, C.-J.; Zevenhoven, R. Fixation of carbon dioxide by producing hydromagnesite from serpentinite. *Appl. Energy* **2009**, *86*, 214–218. [CrossRef]
5. Wang, D.; Li, Z. Gas–Liquid Reactive Crystallization Kinetics of Hydromagnesite in the $MgCl_2$–CO_2–NH_3–H_2O System: Its Potential in CO_2 Sequestration. *Ind. Eng. Chem. Res.* **2012**, *51*, 16299–16310. [CrossRef]
6. Prigiobbe, V.; Hänchen, M.; Werner, M.; Baciocchi, R.; Mazzotti, M. Mineral carbonation process for CO_2 sequestration. *Energy Procedia* **2009**, *1*, 4885–4890. [CrossRef]
7. Zhao, L.; Sang, L.; Chen, J.; Ji, J.; Teng, H.H. Aqueous carbonation of natural brucite: Relevance to CO_2 sequestration. *Environ. Sci. Technol.* **2009**, *44*, 406–411. [CrossRef]
8. IPCC; Masson-Delmotte, V.P.; Zhai, H.-O.; Pörtner, D.; Roberts, J.; Skea, P.R.; Shukla, A.; Pirani, W.; Moufouma-Okia, C.; Péan, R.; et al. Summary for Policymakers. In *Global Warming of 1.5 °C*; An IPCC Special Report on the Impacts of Global Warming of 1.5 °C above Pre-Industrial Levels and Related Global Greenhouse Gas Emission Pathways, in the Context of Strengthening the Global Response to the Threat of Climate Change, Sustainable Development, and Efforts to Eradicate Poverty; World Meteorological Organization: Geneva, Switzerland, 2018; p. 32.
9. Boschi, C.; Dini, A.; Dallai, L.; Ruggieri, G.; Gianelli, G. Enhanced CO_2-mineral sequestration by cyclic hydraulic fracturing and Si-rich fluid infiltration into serpentinites at Malentrata (Tuscany, Italy). *Chem. Geol.* **2009**, *265*, 209–226. [CrossRef]
10. Nirta, G.; Pandeli, E.; Principi, G.; Bertini, G.; Cipriani, N. The Ligurian units of southern Tuscany. *Boll. Soc. Geol. Ital.* **2005**, *3*, 29–54.

11. Langone, A.; Baneschi, I.; Boschi, C.; Dini, A.; Guidi, M.; Cavallo, A. Serpentinite-water interaction and chromium (VI) release in spring waters: Examples from Tuscan ophiolites. *Ofioliti* **2013**, *38*, 41–57.
12. Federici, F. *Relazione Geologico Mineraria sul Giacimento Cuprifero di Montecastelli Pisano*; DBGM: San Giovanni Valdarno, Italy, 1941.
13. Lotti, B. Sul Giacimento Cuprifero di Montecastelli Pisano. In *Bollettino del Reale Comitato Geologico d'Italia XVI*; Reale Comitato Geologico d'Italia: Rome, Italy, 1885.
14. Lotti, B. Rapporto Sulla Miniera Cuprifera di Montecastelli in Toscana. Rapporto interno Montecatini. Società Generale per l'Industria Mineraria e Chimica. 1924. Available online: http://www.neogeo.unisi.it/dbgmnew/ricerca.asp?act=see&id=12922 (accessed on 1 July 2019).
15. Settore Idrologico Regionale (SIR), Regione Toscana. Available online: https://www.sir.toscana.it (accessed on 1 July 2019).
16. Jackson, S.E. LAMTRACE Data Reduction Software for LAICP-MS. In *Laser Ablation ICP-MS in the Earth Sciences: Current Practices and Outstanding Issues*; Sylvester, P., Ed.; Mineralogical Association of Canada: Quebec, QC, Canada, 2008; Volume 40, pp. 305–307, Short Course Series.
17. Parkhurst, D.L.; Appelo, C. User's guide to PHREEQC (Version 2): A computer program for speciation, batch-reaction, one-dimensional transport, and inverse geochemical calculations. *Water Resour. Investig. Rep.* **1999**, *99*, 312.
18. Brindley, G.W.; Bish, D.L.; Wan, H.-M. The nature of kerolite, its relation to talc and stevensite. *Mineral. Magazine* **1977**, *41*, 443–452. [CrossRef]
19. Cathelineau, M.; Caumon, M.-C.; Massei, F.; Brie, D.; Harlaux, M. Raman spectra of Ni-Mg kerolite: Effect of Ni-Mg substitution on O–H stretching vibrations. *J. Raman Spectrosc.* **2015**, *46*, 933–940. [CrossRef]
20. Léveillé, R.J.; Longstaffe, F.J.; Fyfe, W.S. Kerolite in carbonate-rich speleothems and microbial deposits from basaltic sea caves, Kauai, Hawaii. *Clays Clay Miner.* **2002**, *50*, 514–524. [CrossRef]
21. Oze, C.; Fendorf, S.; Bird, D.K.; Coleman, R.G. Chromium Geochemistry of Serpentine Soils. *Int. Geol. Rev.* **2004**, *46*, 97–126. [CrossRef]
22. Fairchild, I.J.; Baker, A. *Speleothem Science. From Process to Past Environments*; Wiley-Blackwells: Hoboken, NJ, USA, 2012; p. 450, Blackwell Quaternary Geoscience Series Book 4.
23. Cigna, A.A. An analytical study of air circulation in caves. *Int. J. Speleol.* **1968**, *3*, 41–54. [CrossRef]
24. James, E.W.; Banner, J.L.; Hardt, B. A global model for cave ventilation and seasonal bias in speleothem paleoclimate records. *Geochem. Geophys. Geosyst.* **2015**, *16*, 1044–1051. [CrossRef]
25. Park, A.-H.A.; Fan, L.-S. CO_2 mineral sequestration: Physically activated dissolution of serpentine and pH swing process. *Chem. Eng. Sci.* **2004**, *59*, 5241–5247. [CrossRef]
26. Sanna, A.; Wang, X.L.; Lacinska, A.; Styles, M.; Paulson, T.; Maroto-Valer, M.M. Enhancing Mg extraction from lizardite-rich serpentine for CO_2 mineral sequestration. *Min. Eng.* **2013**, *49*, 135–144. [CrossRef]
27. Daval, D.; Hellmann, R.; Martinez, I.; Gangloff, S.; Guyot, F. Lizardite serpentine dissolution kinetics as a function of pH and temperature, including effects of elevated pCO_2. *Chem. Geol.* **2013**, *351*, 245–256. [CrossRef]
28. Critelli, T.; Marini, L.; Schott, J.; Mavromatis, V.; Apollaro, C.; Rinder, T.; De Rosa, R.; Oelkers, E.H. Dissolution rate of antigorite from a whole-rock experimental study of serpentinite dissolution from 2 < pH < 9 at 25 °C: Implications for carbon mitigation via enhanced serpentinite weathering. *Appl. Geochem.* **2015**, *61*, 259–271.